ACS Catalysis

Open Access
This article is licensed under CC-BY-NC-ND 4.0

pubs.acs.org/acscatalysis
Research Article

Gas Bubble Stabilization Limits Tetraalkylammonium-Enhanced Hydrogen Evolution

Julia Fernández-Vidal,[⊥] Kathryn J. Vannoy,[⊥] Aleksandr Bashkatov, Dominik Krug, Onno van der Heijden, Detlef Lohse, and Marc T. M. Koper*

Cite This: ACS Catal. 2026, 16, 5796−5804
Read Online

ACCESS | Metrics & More | Article Recommendations | Supporting Information

ABSTRACT: Pt is the most active single-metal HER catalyst in acidic media, but its performance drops sharply in alkaline electrolytes. While recent studies have shown that tetraalkylammonium (TAA^+) cations can enhance alkaline HER by restructuring interfacial water, their role under bubble-forming, high-current conditions remains unclear. Here we show that tetrabutylammonium (TBA^+) exerts a dual, potential-dependent effect on Pt: it boosts HER rates at low overpotentials but suppresses them at higher overpotentials. Using microelectrodes with high-speed imaging, we track microbubble formation, growth and detachment, and find that TBA^+ stabilizes bubbles through adsorption at multiple interfaces, including the electrode and surrounding insulator, leading to persistent surface blockage via pinning and coalescence. Rotating disk electrode measurements confirm that the resulting activity loss originates from mass transport limitations rather than intrinsic kinetics. These findings clarify the role of organic cations in governing gas evolution dynamics and highlight the need to account for interfacial bubble effects when interpreting alkaline HER activity.

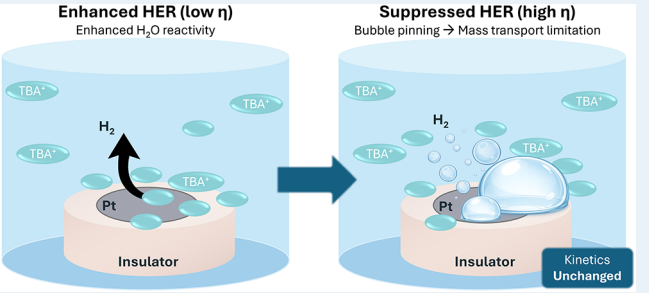

KEYWORDS: *microbubbles, hydrophobic cations, alkaline HER, interfacial adsorption, coalescence*

Downloaded via 84.118.33.72 on March 23, 2026 at 15:03:20 (UTC).
See https://pubs.acs.org/sharingguidelines for options on how to legitimately share published articles.

INTRODUCTION

The hydrogen evolution reaction (HER) on Pt is well understood in acidic media, where Pt exhibits the highest intrinsic activity among single metals due to its exceptional ability to adsorb and recombine reactive hydrogen intermediates (H_{ads}).[1−3] In alkaline media, however, Pt activity is significantly reduced,[4,5] and understanding how the electrolyte composition modifies alkaline HER kinetics remains an open question. In particular, the influence of the solvent and ionic species and their associated interfacial effects has attracted growing attention.[6−9]

Recent work has shown that introducing certain organic species into the electrolyte or onto the electrode surface can enhance HER rates in neutral and alkaline conditions.[10−13] Among these, tetraalkylammonium (TAA^+) cations stand out.[12,14,15] Substituting the canonical sodium (Na^+) or potassium (K^+) for TAA^+ can increase the exchange current density of alkaline HER on Pt by more than a factor of 4.[12] The effect scales with alkyl chain length, consistent with the idea that increased hydrophobicity reorganizes the interfacial water network and facilitates proton-coupled transport.[11,16−19] Similar hydrophobic and amphiphilic effects have also been shown to increase the activity of the oxygen reduction reaction (ORR) in aqueous media,[20−22] and CO_2 reduction in aprotic media.[23]

In our recent work, we showed that tetra-*n*-butylammonium cations (TBA^+), a specific class of TAA^+, form a physisorbed two-dimensional adlayer on Pt electrodes,[15] significantly decreasing the charge associated with the hydrogen underpotential deposition (H_{UPD}) adsorption. Despite the formation of this adlayer, the Pt electrode increases its catalytic activity for HER, associated with hydrogen overpotential deposition (H_{OPD}). This highlights how cation-induced interfacial phenomena can regulate HER activity. However, such studies (including our own work), have been limited to potentials close to the onset of HER (∼−0.1 V_{RHE}), reaching current densities on the order of 1−10 mA/cm^2.[12,15] By contrast, under high-current conditions relevant to fundamental bubble studies, local H_2 supersaturation at the electrodelelectrolyte interface gives rise to gas nucleation, growth, and detachment.[24,25] These processes can strongly influence the apparent catalytic activity.

In this work, we deliberately employ well-defined planar and microelectrode Pt systems to isolate electrolyte-interface

Received: December 15, 2025
Revised: February 10, 2026
Accepted: February 11, 2026
Published: March 10, 2026

© 2026 The Authors. Published by American Chemical Society

interactions and gas bubble dynamics during HER. The simplified geometries used here enable a mechanistic understanding of electrolyte cation effects that would be difficult to resolve in porous catalyst layers. Here, we investigate the effect of TBA^+ on alkaline HER rates over a wider potential range, extending into the high-current regime ($\geq$100 mA/cm^2). We use microelectrodes to isolate interfacial bubble effects. Their small geometry supports only a few micro- or nanobubbles at a given time, making the measured current highly sensitive to bubble dynamics.

This approach builds on extensive prior work where micro- and nanoelectrodes have been used to probe bubble nucleation (nanobubbles),[26] coalescence[27] and detachment.[28] Beyond their bubble-sensitivity, microelectrodes also offer analytical advantages: the radial diffusion profile and steady-state diffusion layer simplify the treatment of mass transport phenomena during gas evolution.

Using this approach, we find that TBAOH enhances HER rates relative to NaOH at low overpotentials ($\geq -0.35 \pm 0.01$ V_{RHE}), in line with the promotional effect reported for TAA^+ cations. However, at higher current densities, this trend reverses, and the HER activity in TBAOH plummets due to bubble accumulation and stabilization at multiple interfaces. By combining electrochemical measurements with high-speed imaging, we disentangle the dual role of TBA^+: while it promotes interfacial water reactivity at low overpotentials, it also creates hydrophobic domains that hinder gas removal at high rates. The electrolyte not only influences catalysis directly but also controls whether bubbles block HER or not, highlighting the need to account for bubble dynamics when evaluating HER activity in alkaline media.

METHODS

General Cleaning

The electrochemical cells were cleaned by immersing them overnight in a 20 mM solution of $KMnO_4$ ($\geq$99.0% Merck). The pH of the solution was set to $\leq$1 with H_2SO_4 (96% Sigma-Aldrich). All the material employed was rinsed with a freshly prepared 10% mixture of H_2SO_4 (96% Sigma-Aldrich) and H_2O_2 (35% Merck) followed by 4–5 rinsing and boiling cycles in ultrapure water (Milli-Q, 18.2 MΩ cm).

Cyclic Voltammetry, Chronoamperometry, and Linear Sweep Voltammetry (LSV)

A standard three-electrode cell assembly and a BioLogic VSP300 potentiostat were employed for the electrochemical measurements. Pt wire (99.9%, Mateck) was used as the counter electrode and a HydroFlex reference electrode (Gaskatel), connected with an additional 10 μF shunt capacitor, was used as reference electrode. Current densities (j) were calculated by normalizing the current to the geometric area of the Pt electrodes. An 85% iR correction was applied using the BioLogic EC-Lab software and the remaining 15% of the iR correction was manually performed during the data analysis. All the potentials in this manuscript are reported vs the RHE scale, 100% iR corrected.

Electrolytes

Fresh 0.1 M NaOH solution (30% Suprapur) and 0.1 M TBAOH (40 wt % in H_2O Sigma-Aldrich) were used as electrolytes (pH 13). The electrolytes were purged with high-purity Ar (N5).

Rotating Disk Electrode (RDE) Preparation

A rotating disk electrode (RDE) setup (MSR rotator, Pine research) was used. The working electrode was a Pt polycrystalline disk with a diameter of 5 mm (99.99% Pine research), embedded in a polyether ether ketone (PEEK) insert. The Pt disk electrode was manually polished on micropolishing cloths with four different diamond suspensions (Buehler) of decreasing particle size (3 μm, 1 μm, 0.25 and 0.05 μm), then rinsed with ethanol and Milli-Q water, and finally sonicated in ethanol for at least 15 min to remove attached diamond particles. Electrochemical polishing was conducted in the range −0.1 V_{RHE} to 1.5 V_{RHE} at 50 mV/s in 0.1 M NaOH for 20–30 cycles until a clean CV was obtained (Figure S1).

Tafel Analysis

Tafel slope analysis was performed similar to what was described previously, where Tafel slopes over a certain number of data points were given vs averaged current density or potential.[29−31] The slope was calculated from HER LSV data at 50 mV/s over small potential ranges of seven data points. Starting from the first seven points, we shifted down by one point each time to calculate new slopes, moving progressively down the data set. The Tafel slopes (in mV/dec) are obtained from the linear fit of the overpotentials vs log(j), where j is the current density in mA/cm^2.

Microelectrodes Preparation

Pt microelectrodes (Ø10–25 μm) were purchased from CH Instruments. Larger-diameter Pt microelectrodes (Ø25 μm) were fabricated in house by pushing a Pt wire (99.99% Goodfellow) in a glass capillary (1.12 mm inside diameter, Hilgenberg) and heating it in the middle with a butane torch until the capillary melted, breaking into two (with one sealed end and one unsealed end), as described elsewhere.[32] One end of a tungsten wire from GoodFellow (Ø0.5 mm, 99.95% purity) was dipped in Agar Silver Paint (Agar Scientific) and pushed into the open end of each capillary to make the connection with the Pt wire. When the connection was formed, the tungsten was sealed in place with hot Limpatroner glue dispensed with a hot glue gun. The other end was then sanded in Milli-Q water on a P 600 to P 2500 grit sandpaper from HERMES until a flat disk of Pt was apparent in microscopy.

A Nikon OPTIPHOT inverted microscope with 5×, 10×, 20×, and 40× magnifications was used to optically characterize the electrode at all stages in preparation. Optical characterization was primarily done to ensure a proper seal between the metal and the glass, ensure a good electrical connection between the tungsten and Pt, and to verify flatness and cleanliness of the electrode surface. The electrode surface was then smoothed by polishing on micropolishing cloths (Buehler) with diamond suspensions (Buehler) of decreasing particle size (6 μm, 3 μm, 1 μm, 0.25 μm, and 0.05 μm). The polishing was first performed on a Forcipol 1 polishing wheel from Metkon, and after appearing smooth in the microscope, was subsequently manually polished with figure-8 motions and 0.05 μm diamond suspension and then on a clean micropolishing cloth pad with Milli-Q water. Before each use, the surface of the electrode was manually polished as described and checked visually using an optical microscope. Figure S2 shows a micrograph of an acceptable electrode surface taken before electrochemical data collection.

For microelectrodes, slight differences in the current density values are expected among replicates due to differences in surface roughness caused when polishing the electrode surface, as illustrated in Figure S3.

Methylation of Microelectrodes

To directly assess the impact of a hydrophobic insulator (glass) surface, the glass on the Pt microelectrodes was methylated by dipping the exposed Pt end of the microelectrode in a prepared solution of 5% dimethyldichlorosilane (Sigma, 99+%) in toluene (Sigma, anhydrous 99.8%) for ∼30 s. The electrode was then thoroughly rinsed with ethanol and water before use. Micrographs of a glass slide with and without the silane treatment show that the contact angle of a 5 μL droplet of 100 mM NaOH solution is 90 and 46, respectively (Table S1), demonstrating higher hydrophobicity of the glass after being methylated.

Optical Imaging

To analyze the dynamics of H_2 bubbles, additional LSV measurements were performed simultaneously with image recording using a three-electrode electrochemical cell and a shadowgraphy system. The

https://doi.org/10.1021/acscatal.5c08904
ACS Catal. 2026, 16, 5796−5804

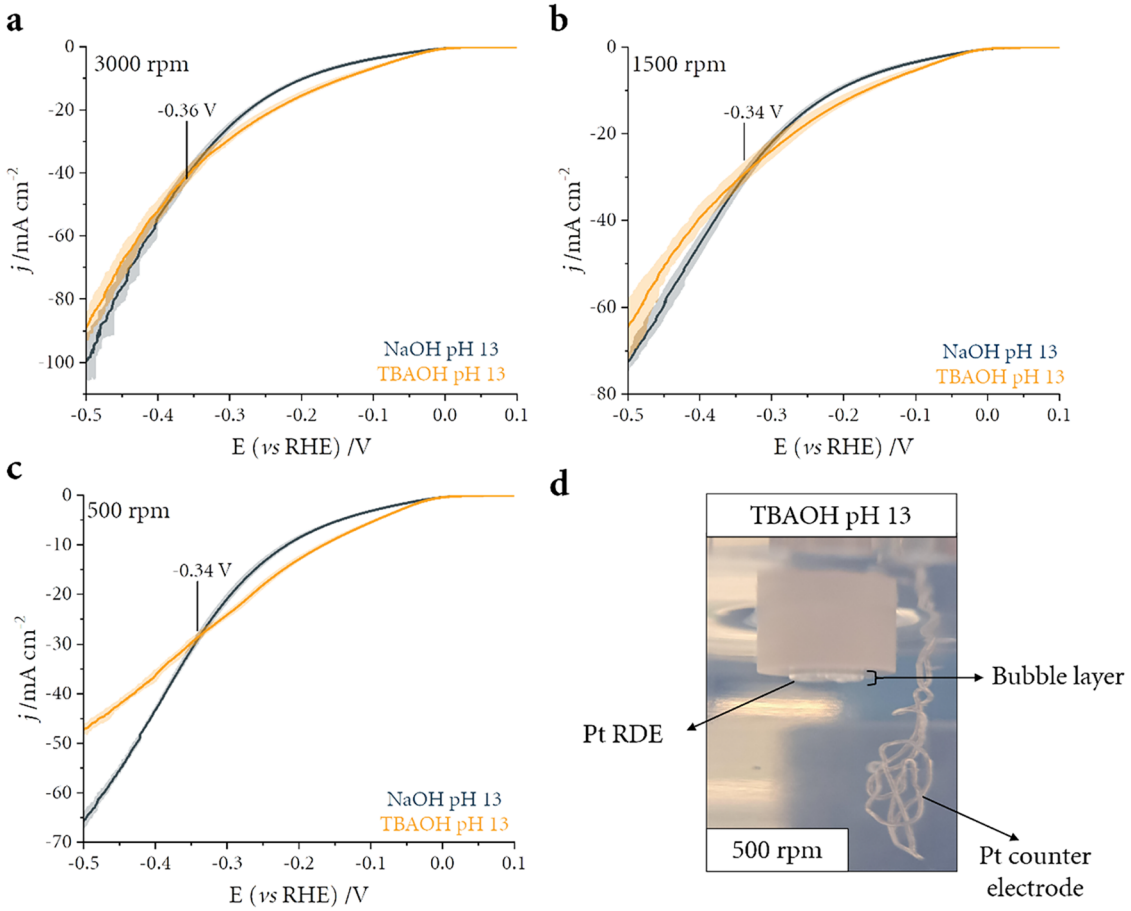

Figure 1. (a–c) Linear sweep voltammograms of Pt RDE in NaOH pH 13 (gray) and in TBAOH pH 13 (yellow) during HER at 3000 rpm (a), 1500 rpm (b), and 500 rpm (c). The scan rate was 50 mV/s. The HER currents have been averaged with 2–4 replicates and the standard deviation is displayed as a shade around the line. Currents have been normalized by the geometrical area of the electrode and potentials have been *iR* corrected. (d) Optical photography taken from RDE electrode rotating at 500 rpm in TBAOH pH 13.

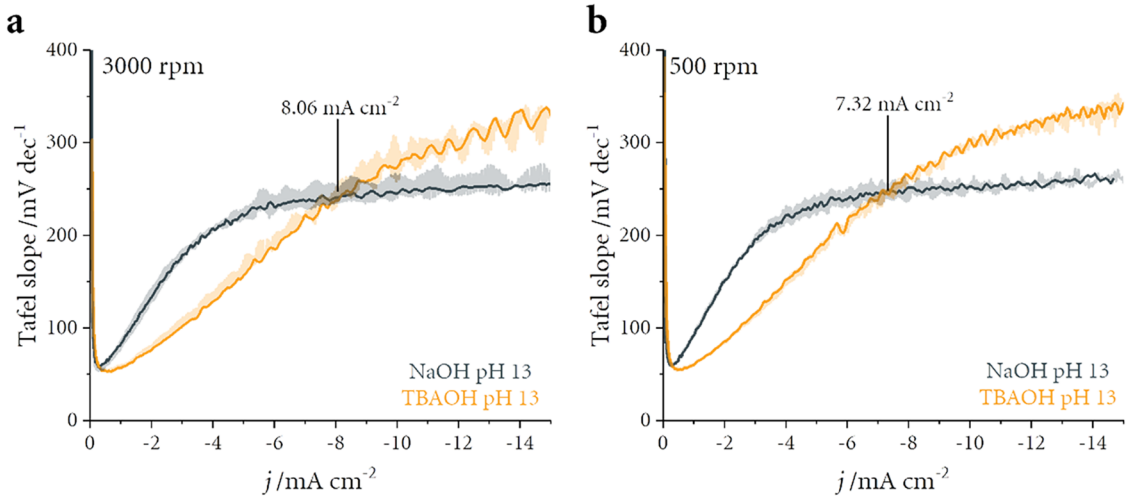

Figure 2. Tafel slope plots of the HER vs averaged current density on Pt RDE in NaOH pH 13 (gray) and in TBAOH pH 13 (yellow) at 3000 rpm (a), and 500 rpm (b). The Tafel slope values have been calculated with the LSV data displayed in Figure 1a and 1c. The standard deviation is displayed as a shade around the line.

electrochemical cell consisted of a Ø10 μm Pt microelectrode (working electrode) facing upward, at the base of a cuboid glass cuvette (Hellma, 10 × 10 × 40 mm^3). The cuvette was cleaned following the *General cleaning* employed for all electrochemical cells. The cuvette, filled with either 0.1 M NaOH or 0.1 M TBAOH, was completed by a counter electrode (Ø0.5 mm Pt wire 99.9%) and a reference electrode Ag/AgCl, both inserted vertically from the top. The potential was controlled using a potentiostat (BioLogic VSP300).

Bubble dynamics were visualized from two perpendicular side views, using a shadowgraphy system. The system consisted of two

https://doi.org/10.1021/acscatal.5c08904
ACS Catal. 2026, 16, 5796–5804

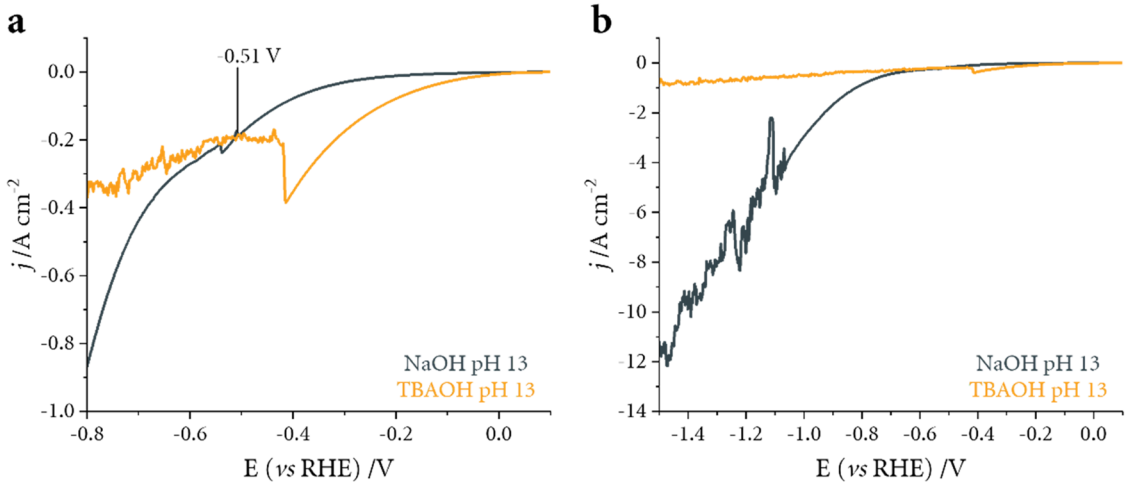

Figure 3. Linear sweep voltammograms of Pt microelectrode Ø25 μm in NaOH pH 13 (gray) and in TBAOH pH 13 (yellow) during HER (a) between 0.1 V_{RHE} to −0.8 V_{RHE}, and (b) between 0.1 V_{RHE} to −1.5 V_{RHE}. Scan rate 50 mV/s. Currents have been normalized by the geometrical area of the electrode.

high-speed cameras (#1: Photron, FASTCAM NOVA S16 and #2: Photron, FASTCAM NOVA S12). Camera #1 was equipped with a long-distance zoom lens system (Navitar, 12X), while camera #2 was connected to an optical microscope with a long-distance objective (Olympus, SLMPLN 20X), providing spatial resolution of 708 pix/mm and 996 pix/mm, respectively. The system is completed with two backlight LED illumination (SCHOTT, KL 2500), one for each camera. Image recording was performed at 125 frames/s.

Optical images in Figures 1d and S10 were taken with a mobile phone iPhone XS.

RESULTS AND DISCUSSION

Tetraalkylammonium cations (TAA^+) have been shown to enhance hydrogen evolution reaction (HER) kinetics on Pt polycrystalline[12] and single-crystal[11,15] electrodes in alkaline media, particularly at low overpotentials (<−0.2 V_{RHE}). Linear sweep voltammograms (LSVs) obtained in NaOH and TBAOH electrolytes at various rotation rates are shown in Figure 1a−c. At low overpotentials, the expected HER promotion by TBA^+ is observed, consistent with previous reports. However, at higher overpotentials (≥−0.35 ± 0.01 V_{RHE}), this trend reverses and NaOH shows significantly higher current densities. This crossover suggests that the factor limiting HER performance changes as the potential becomes more negative. The small shift in this crossover potential (≈20 mV between 500 and 3000 rpm), further suggests that these differences originate from changes in mass-transport rather than intrinsic reaction kinetics.

Direct visual observation supports this interpretation. At low rotation rates (500 rpm) we could visually observe the formation of a persistent bubble layer on the electrode surface (Figure 1d). This indicates that the transition from HER promotion to suppression in the presence of TBA^+ arises from increased bubble stability. The effect was consistent across all rotation rates studied and became more pronounced at lower rotation speeds. Importantly, suppression of HER activity by TBA^+ remained even at the highest rotation rates tested, showing that typical forms of forced convection cannot fully overcome these interfacial effects.

To corroborate these observations and assess how bubble accumulation manifests in the electrochemical response, we performed a Tafel analysis of the RDE data (Figure 2). In both NaOH and TBAOH, the Tafel slopes are low at small currents but increase sharply with current density, consistent with a transition from kinetically controlled HER to regimes dominated by mass transport or bubble effects. The initial slopes and onset of this transition are similar in both electrolytes, indicating that the underlying HER mechanism is unchanged by replacing Na^+ with TBA^+. At higher currents (and high overpotentials-see Figure S4), however, the apparent slope in TBAOH surpasses that in NaOH, reflecting stronger bubble-induced inhibition that persists even under high rotation rates. Notably, the slope crossover occurs at progressively higher current densities when the rotation rate is increased (7.30 mA cm^{-2} at 500 rpm vs 8.06 mA cm^{-2} at 3000 rpm). This behavior confirms that forced convection delays bubble accumulation at the electrode surface, but cannot prevent it entirely, as stabilized bubbles in TBAOH eventually dominate the response. Thus, the divergence between the two electrolytes cannot be explained by intrinsic kinetics but instead by interfacial bubble dynamics.

It is visually apparent that bubble behavior differs strongly between NaOH and TBAOH (Figure 1d), with bubble retention in the latter correlating directly with the decrease in HER activity. However, the direct role of TBA^+ within the newly formed multiphase microenvironment (bubbleelectrolytelsurface) remains difficult to resolve at this scale. To disentangle these contributions, we next turned to microelectrodes. Their small size allows one to correlate sudden drops in current density with partial blockages of the surface. Because the surfaces are on the order of ten microns in diameter, the current can report on the behavior of micron-sized bubbles. This approach provides a more direct view of how TBA^+ alters bubble nucleation, growth, and detachment, and ultimately how these effects govern the balance between promotion and suppression across the HER potential window.

LSVs in NaOH and TBAOH solutions at pH 13 (Figure 3) show a clear promotional effect of HER at low overpotentials in TBAOH (Figure 3a), consistent with previous results in macroelectrodes (see Figure S5 for Tafel analysis).[12,15] High-resolution current traces reveal a sharp decrease in current (Figure 3a) in TBAOH. This sharp drop (yellow line at around −0.42 V_{RHE}), previously observed for both nano-[26,33−36] and microelectrodes[27,28,37,38] is attributed to the formation of gas bubbles at the electrode surface after the local concentration of

https://doi.org/10.1021/acscatal.5c08904
ACS Catal. 2026, 16, 5796−5804

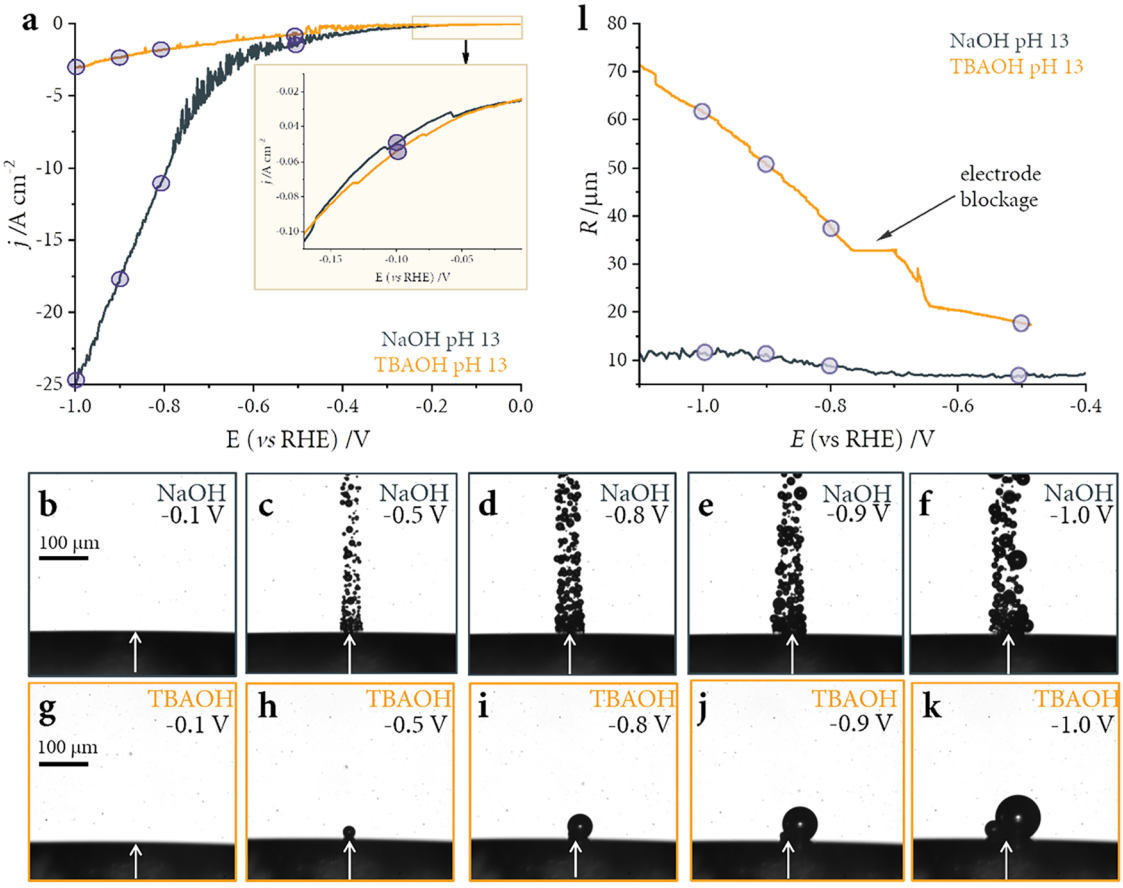

Figure 4. (a) Linear sweep voltammograms of Pt microelectrode Ø10 μm in NaOH pH 13 (gray) and in TBAOH pH 13 (yellow) during HER. Scan rate 50 mV/s. Currents have been normalized by the geometrical area of the electrode. (b–k) Snap images of H_2 bubble formation and detachment during LSV in NaOH pH 13 (b-f) and TBAOH pH 13 (g–k). The arrows represent the position of the Pt microelectrode. (l) Quantification of bubble size measured from the high-speed imaging data shown in panels (b–k). The bubble radius was extracted from the optical frames and plotted as a function of potential for NaOH (gray) and TBAOH (yellow).

dissolved H_2 near the electrode exceeds the nucleation thresholds. Each discrete current drop observed in the LSV corresponds to the optical appearance of one or multiple new bubble(s) on the electrode surface (Figure S6), confirming that the electrochemical signal directly reports on bubble formation and detachment.

To further investigate bubble behavior in more detail, we combined electrochemical measurements with a shadowgraphy system (Figure 4). A Ø10 μm Pt microelectrode was positioned facing upward at the bottom of the electrochemical cell, allowing buoyancy to assist in bubble detachment from the electrode surface. Control experiments with microelectrodes oriented both up- and downward showed similar results (see Figure S7). We chose smaller microelectrodes to reduce the number of bubbles on the surface, giving a clearer picture of microbubble dynamics. Unlike previous studies using nanoelectrodes where bubble-formation current transients were analyzed to determine the nucleation threshold,[26,33−35] our studies with microelectrodes focus instead on the evolution, growth, and detachment of bubbles. Single nucleation events are not clearly observable here, most likely because multiple nucleation sites form across the microelectrode surface (as suggested by the dense layer of microbubbles that appears after HER begins).[27,39]

Figure 4a shows an overlay of LSVs recorded in TBAOH and in NaOH using a Ø10 μm Pt microelectrode. The corresponding snapshots in Figure 4b–k, taken at the specific potentials marked by circles in Figure 4a, illustrate significant differences in H_2 bubble behavior between the two electrolytes, despite their nearly identical pH (13 ± 0.1).

HER in NaOH (Figure 4b–f) proceeds via a continuous release of microbubbles, which appear in the microscopy images around −0.27 V_{RHE} (see Figure S8 for the simultaneously recorded images from the front- and side-view images of the cell). The average bubble radius increases progressively as the overpotential rises. In contrast, HER in TBAOH (Figure 4g–k) is dominated by the growth of a single, much larger, and persistent microbubble that continuously grows as the overpotential is increased (Figure 4l). Shortly after nucleation, the primary growing H_2 bubble migrates laterally and pins to the insulating glass surrounding the Pt disk (see Figure S9), where it remains anchored through the entire LSV. Rather than detaching, the bubble grows mainly through coalescence with newly formed microbubbles at the electrode surface, reaching a radius of 165 μm by the end of the forward scan (−2.5 V_{RHE}) and expanding further to 215 μm during the reverse scan. Notably, no bubble detachment is observed at any stage (Supporting Videos S1–S4), highlighting the extreme stability of the pinned bubble and the profound influence of interfacial interactions on gas evolution dynamics.

We suggest that the markedly different bubble behavior observed in TBAOH compared to NaOH arise mainly from

https://doi.org/10.1021/acscatal.5c08904
ACS Catal. 2026, 16, 5796−5804

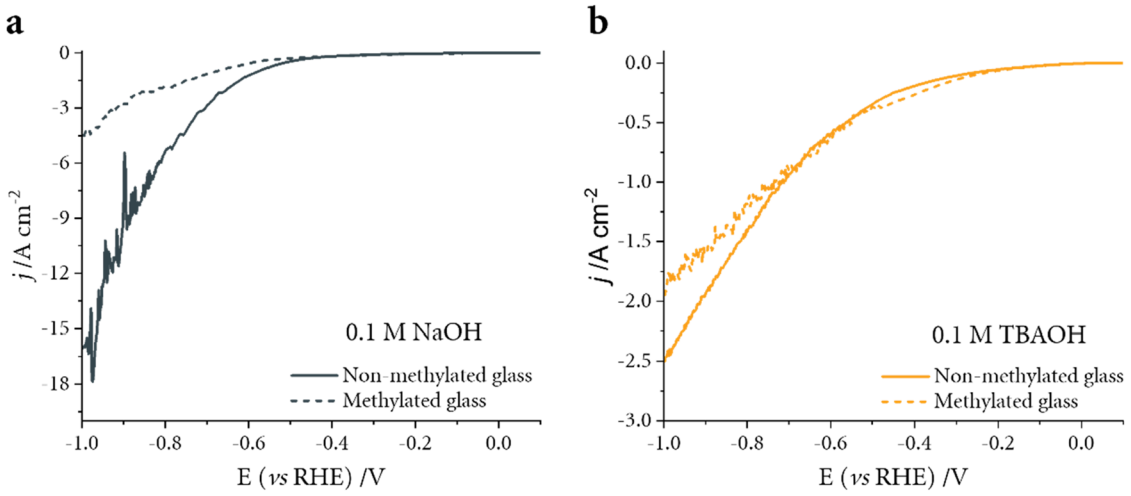

Figure 5. LSVs of Pt microelectrodes Ø100 μm in (a) NaOH pH 13 and (b) TBAOH pH 13 during HER. The glass surrounding the Pt microelectrode was untreated (solid line) and methylated with dimethyldichlorosilane (dashed line). Scan rate 50 mV/s. Currents have been normalized by the geometrical area of the electrode.

two interrelated interfacial phenomena: (1) enhanced bubble coalescence, and (2) stronger pinning forces. Both effects are likely driven by the adsorption of TBA^+ at various interfaces (See Figure S10 for a schematic representation of the different interfaces). In the following section, we place these observations within established mechanistic frameworks to highlight how specific cation effects at interfaces can profoundly influence gas evolution behavior.

Enhanced Coalescence in TBAOH

In TBAOH, larger bubbles are observed compared to bubbles in NaOH, a trend attributed to a more efficient coalescence. The bubble sizes observed in NaOH fall within the range typically reported for alkaline HER,[40] confirming that our system behaves consistently with previous studies and that the differences observed in TBAOH arise from electrolyte-specific effects rather than experimental artifacts. At pH 13, bubbles carry a net negative surface charge, which would normally promote electrostatic repulsion and hinder coalescence. However, previous reports[41] have shown that TBA^+ can adsorb at the bubblelelectrolyte interface due to a combination of electrostatic attraction between the cation and the negatively charged bubble (at pH 13),[42,43] and hydrophobic interactions.[44] This adsorption likely screens part of the negative charge, reducing bubble−bubble repulsion and facilitating coalescence.

Additionally, the increased hydrophobicity of the bubblel electrolyte interface in alkaline conditions may promote hydrophobic interactions between adjacent TBA^+ layers on neighboring bubbles, further enhancing coalescence.[45] This behavior can also be understood following the empirical classification of ions by Craig et al.,[46] which extends the Hofmeister series to describe electrolyte effects on bubble coalescence.[28,47] According to this, electrolytes composed of similar ion types (either $\alpha\alpha$ or $\beta\beta$ combinations) tend to inhibit bubble coalescence, whereas mixed $\alpha\beta$ or $\beta\alpha$ combinations allow bubbles to merge more easily. TBA^+ are considered as β-type (chaotropic) cations due to their large size and weak hydration, in contrast to small alkali metal cations such as Na^+ or K^+, which are α-type (kosmotropic). In our case, the combination of β-type TBA^+ with α-type OH^- forms an $\alpha\beta$ electrolyte, which, according to Craig's classification, favors coalescence. This is fully consistent with our observations that TBA^+ promotes bubble merging and stabilizes larger bubbles at the interface through interfacial adsorption.

The effect is reinforced by the substantially lower surface tension of TBAOH ($\gamma \approx 50-55$ mN/m)[48] compared to NaOH ($\gamma \approx 72$ mN/m)[49] which has been linked to the formation of larger bubbles.[50] Together, charge screening, hydrophobic interactions, and reduced surface tension provide a coherent explanation for the enhanced coalescence observed in TBAOH. It is worth noting that this behavior contrasts with reports in acidic media, where reduced coalescence has been observed.[51] While we anticipate that there is a role of the chosen anion/cation pairs in the specific studies,[28,51] in acidic media (below pH 3), bubbles have a positive charge due to the adsorption of hydronium (H_3O^+),[42] which likely leads to differences in TBA^+ interaction at these boundaries.[51] The reversal of this trend in alkaline TBAOH underscores the electrolyte-specific role of TBA^+ in modulating interfacial forces and, ultimately, bubble dynamics.

Pinning Forces and Bubble Adhesion

At high overpotentials, HER in TBAOH exhibits unusually stable bubbles that detach far less readily compared to those in NaOH. We attribute this effect to the appearance of additional downward pinning forces due to the bubble adhesion at the glass (or electrode) surface and respective formation of the contact line. Our previous study[15] showed that TBA^+ forms a physisorbed adlayer on Pt and interacts more strongly in the presence of OH_{ads} species, providing direct spectroscopic support for the adsorption mechanism proposed here. It is important to note that TBA^+ physisorption is reversible and potential-dependent, consistent with an interfacial electrolyte effect rather than a persistent surface alteration. Physisorption of TBA^+ at the Ptlelectrolyte interface[15] increases interfacial hydrophobicity, which promotes the accommodation of gas bubbles on the electrode surface. Previous studies have further shown that, while smaller TAA^+ do not detectably adsorb to the interface, TBA^+ can penetrate hydrophobic phases.[44] This penetration of the alkyl chains into the bubble hydrophobic (gas) phase may contribute to the observed bubble stabilization on the Pt surface.

https://doi.org/10.1021/acscatal.5c08904
ACS Catal. 2026, 16, 5796−5804

We must also address that, especially as bubbles grow beyond the microelectrode radius, eventually becoming nearly 100 times larger, the role of the surrounding glass insulator also becomes critical. Under alkaline conditions, the glass|electrolyte interface is expected to carry a negative charge, making TBA^+ adsorption favorable. We suggest that this adsorption increases the hydrophobicity of the glass surface, explaining why bubbles nucleated at the electrode or at the electrode|glass boundary often migrate laterally and pin to the glass. This effect may even outweigh adsorption on Pt, where strong molecular fluxes and convective flow continually disturb the interfacial layer.

Bubble attachment to a surface adds an additional capillary force due to the contact line between the bubble and the electrode and/or surrounding glass. Strong evidence for contact line formation is the fact that bubbles in TBAOH remain pinned even after the LSV is completed, when both Marangoni and electric forces have vanished.[28,39] The contact line retains small bubbles in place long after these forces dissipate, delaying bubble detachment (i.e., until the buoyancy is sufficient to overcome the stabilizing forces). This behavior contrasts with the more common scenario of bubble evolution on a microelectrode,[27,28,38] including in NaOH electrolyte at high currents (see Supporting Videos S1−S4), where the growing bubble rests on a "carpet" of smaller microbubbles without true pinning, and is retained predominantly by electric and Marangoni forces. Recent work has demonstrated that a transition from "carpet"-supported to directly pinned bubbles can occur, depending on the electrode morphology and electrolyte composition, both of which modulate the balance of Marangoni forces.[39]

To disentangle the effect of hydrophobic changes from the glass and electrode surfaces, we modified the insulating glass with dimethyldichlorosilane, creating a methylated, hydrophobic surrounding surface (Figure 5). In NaOH, this methylation led to a pronounced decrease in HER current density (Figure 5a). Correlated microscopy confirmed that the hydrophobized glass impeded the removal of microbubbles from the microelectrode surface (Figure S11). In TBAOH, the reduction in current density is less pronounced (Figure 5b), consistent with the idea that TBA^+ adsorption already renders the glass surface hydrophobic, even before the silane treatment. Together, these results confirm that the hydrophobicity of the surrounding insulator plays a significant role in the observed current at bubble-forming overpotentials. While the influence of the glass is most often neglected, this has been observed before with other hydrophobic phase interactions.[36,52]

Taken together, these findings show that electrolyte composition cannot be viewed solely by its effect on catalytic activity; instead, it fundamentally reshapes the entire multiphase environment of the electrode. In the case of TBA^+, the same adsorption phenomena that enhances water reactivity at low overpotentials becomes detrimental under vigorous gas evolution, where stabilized bubbles dominate the interface. This dual behavior highlights the importance of evaluating electrocatalysts across wider potential and current density ranges, where the balance between intrinsic activity and bubble-driven mass transport phenomena can change dramatically.

More broadly, our results highlight that bubble dynamics, often regarded as a secondary or purely engineering concern, are inseparably linked to interfacial chemistry. We demonstrate that physisorbed cations can control not only catalytic turnover but also bubble coalescence, pinning, and detachment. In other words, tuning the interface is a powerful way to control and improve gas-evolving reactions. Future strategies will need to combine catalytic promotion with controlled bubble management, moving beyond the idea of universally "hydrophobic" or "hydrophilic" interfaces. Instead, interfaces should be tailored to the specific conditions in which the reaction takes place, particularly in nanostructured or porous catalyst layers where confinement and local hydrophobic domains may strongly amplify bubble-retention effects.

CONCLUSIONS

This study reveals a dual, potential-dependent role of tetrabutylammonium (TBA^+) in the alkaline HER on Pt. At low overpotentials, TBA^+ physisorption on Pt enhances HER activity by restructuring interfacial water, whereas at higher current densities the same interfacial hydrophobicity stabilizes bubbles, leading to persistent surface blockage through pinning and coalescence. Microelectrode experiments combined with high-speed microscopy reveal that this crossover originates from H_2 bubble retention at both the electrode surface and the electrode|insulator boundary in TBAOH. Rotating disk electrode studies confirm that the suppression persists even under strong convection, highlighting that bubble stabilization, not catalytic deactivation, governs performance at high rates.

Our findings show that bulky, hydrophobic cations are prone to adsorb at multiple phase boundaries (electrode|electrolyte, bubble|electrolyte, and insulator|electrolyte) reshaping interfacial properties and reducing reaction efficiency by inhibiting bubble detachment. Thus, interfacial hydrophobicity is not inherently beneficial or detrimental: it promotes reactivity when gas evolution is limited, but suppresses activity once vigorous bubble formation dominates.

Although our experiments were carried out under controlled conditions, the interfacial mechanisms revealed here show that tuning surface/interfacial hydrophobicity (through tailored additives, coatings, or support materials) could help manage bubble behavior and gas removal, offering new ways to enhance mass transport and efficiency in real devices. The results also highlight several practical considerations: (i) catalyst performance should extend to industrially relevant potentials where bubble formation and detachment becomes rate-limiting, and (ii) microelectrode studies should account for possible effects of the surrounding insulator on bubble pinning. Finally, our findings indicate that hydrophobic salts such as TBA^+, while enhancing HER kinetics at low overpotentials, are unlikely to improve performance under high-current, bubble-evolving conditions. This perspective, often overlooked in the literature, emphasizes that hydrophobic domains near a catalyst can dominate bubble retention. Looking forward, we recommend further investigation into how exposed or aging catalyst supports influence bubble retention and gas removal, as such effects may significantly impact the apparent activity of these electrodes.

ASSOCIATED CONTENT

Supporting Information

The Supporting Information is available free of charge at https://pubs.acs.org/doi/10.1021/acscatal.5c08904.

Electrochemical characterization, control experiments, and visual analyses that complement the main findings; this includes cyclic voltammograms in NaOH and

https://doi.org/10.1021/acscatal.5c08904
ACS Catal. 2026, 16, 5796−5804

TBAOH (Figure S1), microelectrode surface imaging (Figure S2), and replicate voltammograms highlighting microelectrode surface variability (Figure S3); contact angle measurements on methylated vs untreated glass that reveal differences in electrolyte-surface interactions (Table S1); Tafel slope analyses at various electrode types and rotation speeds (Figures S4−S5) to support the discussion on HER kinetics; a series of figures (Figures S6−S11) to document hydrogen bubble formation and dynamics under different conditions, as well as the influence of electrode orientation and glass surface treatment; Note 1 and Figure S12 provide mechanistic insight into the potential-dependent effects of TBA^+ on HER current density; bubble dynamics are further illustrated in Supporting Videos S1−S4 (PDF)

AUTHOR INFORMATION

Corresponding Author

Marc T. M. Koper − *Leiden Institute of Chemistry, Leiden University, 2300 RA Leiden, The Netherlands;* orcid.org/0000-0001-6777-4594; Email: m.koper@lic.leidenuniv.nl

Authors

Julia Fernández-Vidal − *Leiden Institute of Chemistry, Leiden University, 2300 RA Leiden, The Netherlands*

Kathryn J. Vannoy − *Leiden Institute of Chemistry, Leiden University, 2300 RA Leiden, The Netherlands;* orcid.org/0000-0002-5723-9755

Aleksandr Bashkatov − *Physics of Fluids Group, Max Planck Center for Complex Fluid Dynamics, University of Twente, 7500 AE Enschede, The Netherlands; Institute of Aerodynamics and Chair of Fluid Mechanics, RWTH Aachen University, 52062 Aachen, Germany*

Dominik Krug − *Physics of Fluids Group, Max Planck Center for Complex Fluid Dynamics, University of Twente, 7500 AE Enschede, The Netherlands; Institute of Aerodynamics and Chair of Fluid Mechanics, RWTH Aachen University, 52062 Aachen, Germany;* orcid.org/0000-0002-0627-5676

Onno van der Heijden − *Leiden Institute of Chemistry, Leiden University, 2300 RA Leiden, The Netherlands*

Detlef Lohse − *Physics of Fluids Group, Max Planck Center for Complex Fluid Dynamics, University of Twente, 7500 AE Enschede, The Netherlands; Max Planck Institute for Dynamics and Self-Organization, Göttingen 37077, Germany;* orcid.org/0000-0003-4138-2255

Complete contact information is available at: https://pubs.acs.org/10.1021/acscatal.5c08904

Author Contributions

[⊥]J.F.-V. and K.J.V. contributed equally to this work. Conceptualisation: J.F.-V. and K.J.V. Methodology: J.F.-V., K.J.V, A.B, and O.v.d.H. Investigation: J.F.-V., K.J.V. and A.B. Visualization: J.F.-V. and K.J.V. Funding acquisition: M.T.M.K. Project administration: M.T.M.K. Supervision: D.K., D.L., and M.T.M.K. Writing the original draft: J.F.-V. and K.J.V. Review & editing: J.F.-V., K.J.V., A.B., O.v.d.H., D.K., D.L., and M.T.M.K. All authors have given approval to the final version of the manuscript.

Notes

The authors declare no competing financial interest.

ACKNOWLEDGMENTS

This work was funded by the European Research Council (ERC), Advanced Grant No. 101019998 "FRUMKIN". D.L. and D.K. received funding from the Advanced Research Center Chemical Building Blocks Consortium (ARC CBBC), under the project of New Chemistry for a Sustainable Future (project number 2021.038.C.UT.14). O.v.d.H. acknowledges the funding provided by the Dutch Research Council (NWO) as part of the Reversible Large Scale Energy Storage (RELEASE) consortium (project number 17621).

REFERENCES

(1) Rebollar, L.; Intikhab, S.; Oliveira, N. J.; et al. "Beyond Adsorption" Descriptors in Hydrogen Electrocatalysis. *ACS Catal.* **2020**, *10*, 14747−14762.

(2) Hansen, J. N.; Prats, H.; Toudahl, K. K.; et al. Is There Anything Better than Pt for HER? *ACS Energy Lett.* **2021**, *6*, 1175−1180.

(3) Markovića, N. M.; Sarraf, S. T.; Gasteiger, H. A.; Ross, P. N. Hydrogen Electrochemistry on Platinum Low-Index Single-Crystal Surfaces in Alkaline Solution. *J. Chem. Soc., Faraday Trans.* **1996**, *92*, 3719−3725.

(4) Sheng, W.; Gasteiger, H. A.; Shao-Horn, Y. Hydrogen Oxidation and Evolution Reaction Kinetics on Platinum: Acid vs Alkaline Electrolytes. *J. Electrochem. Soc.* **2010**, *157*, No. B1529.

(5) Briega-Martos, V.; Ferre-Vilaplana, A.; Herrero, E.; Feliu, J. M. Why the activity of the hydrogen oxidation reaction on platinum decreases as pH increases. *Electrochim. Acta* **2020**, *354*, No. 136620.

(6) Goyal, A.; Koper, M. T. M. The Interrelated Effect of Cations and Electrolyte pH on the Hydrogen Evolution Reaction on Gold Electrodes in Alkaline Media. *Angew. Chem., Int. Ed.* **2021**, *60*, 13452−13462, DOI: 10.1002/anie.202102803.

(7) Goyal, A.; Louisia, S.; Moerland, P.; Koper, M. T. M. Cooperative Effect of Cations and Catalyst Structure in Tuning Alkaline Hydrogen Evolution on Pt electrodes. *J. Am. Chem. Soc.* **2024**, *146*, 7305−7312.

(8) Monteiro, M. C. O.; Goyal, A.; Moerland, P.; Koper, M. T. M. Understanding Cation Trends for Hydrogen Evolution on Platinum and Gold Electrodes in Alkaline Media. *ACS Catal.* **2021**, *11*, 14328−14335.

(9) Yu, X.; Zhao, J.; Zheng, L. R.; et al. Hydrogen Evolution Reaction in Alkaline Media: Alpha- or Beta-Nickel Hydroxide on the Surface of Platinum? *ACS Energy Lett.* **2018**, *3*, 237−244.

(10) Uchida, T.; Sasaki, Y.; Ikeshoji, T.; Osawa, M. 4, 4′-Bipyridine as a molecular catalyst for electrochemical hydrogen production. *Electrochim. Acta* **2017**, *248*, 585−592.

(11) Tanaka, S.; Takaya, S.; Kumeda, T.; et al. Tailoring the hydrophilic and hydrophobic reaction fields of the electrode interface on single crystal Pt electrodes for hydrogen evolution/oxidation reactions. *Int. J. Hydrogen Energy* **2021**, *46*, 28078−28086.

(12) Zhao, K.; Yu, H.; Xiong, H.; et al. Action at a distance: organic cation induced long range organization of interfacial water enhances hydrogen evolution and oxidation kinetics. *Chem. Sci.* **2023**, *14*, 11076−11087.

(13) Zhao, K.; Xiang, N.; Wang, Y. Q.; et al. A molecular design strategy to enhance hydrogen evolution on platinum electrocatalysts. *Nat. Energy* **2025**, *10*, 725−736, DOI: 10.1038/s41560-025-01754-4.

(14) Wandlowski, T.; de Levie, R. Double-layer dynamics in the adsorption of tetrabutyl ammonium ions at the mercury-water interface II: Capacitance transients. *J. Electroanal. Chem.* **1993**, *345*, 413−432.

(15) Fernández-Vidal, J.; Koper, M. T. M. Effect of a Physisorbed Tetrabutylammonium Cation Film on Alkaline Hydrogen Evolution Reaction on Pt Single-Crystal Electrodes. *ACS Catal.* **2024**, *14*, 8130−8137.

(16) Stangret, J.; Gampe, T. Hydration sphere of tetrabutylammonium cation. FTIR studies of HDO spectra. *J. Phys. Chem. B* **1999**, *103*, 3778−3783.

(17) Sun, Q.; Oliveira, N. J.; Kwon, S.; et al. Understanding hydrogen electrocatalysis by probing the hydrogen-bond network of water at the electrified Pt−solution interface. *Nat. Energy* **2023**, *8*, 859−869.
(18) Marcus, Y. Tetraalkylammonium ions in aqueous and non-aqueous solutions. *J. Solution Chem.* **2008**, *37*, 1071−1098.
(19) Marcus, Y. Thermodynamics of solvation of ions. Part 5.—Gibbs free energy of hydration at 298.15 K. *J. Chem. Soc., Faraday Trans.* **1991**, *87*, 2995−2999.
(20) Hoshi, N.; Nakamura, M. Enhancement of the Activity for the Oxygen Reduction Reaction on Well-defined Single Crystal Electrodes of Pt by Hydrophobic Species. *Chem. Lett.* **2021**, *50*, 72−79.
(21) Hoshi, N.; Nakamura, M.; Kubo, R.; Suzuki, R. Enhanced oxygen reduction reaction on caffeine-modified platinum single-crystal electrodes. *Commun. Chem.* **2024**, *7*, No. 23.
(22) Kumeda, T.; Tajiri, H.; Sakata, O.; Hoshi, N.; Nakamura, M. Effect of hydrophobic cations on the oxygen reduction reaction on single−crystal platinum electrodes. *Nat. Commun.* **2018**, *9*, No. 4378, DOI: 10.1038/s41467-018-06917-4.
(23) McGregor, J.-M.; Bender, J. T.; Petersen, A. S.; et al. Organic electrolyte cations promote non-aqueous CO2 reduction by mediating interfacial electric fields. *Nat. Catal.* **2025**, *8*, 79−91.
(24) Hydrogen Europe Strategic Research and Innovation Agenda 2021−2027 2022.
(25) Schmidt, O.; Gambhir, A.; Staffell, I.; et al. Future cost and performance of water electrolysis: An expert elicitation study. *Int. J. Hydrogen Energy* **2017**, *42*, 30470−30492.
(26) Chen, Q.; Luo, L.; Faraji, H.; Feldberg, S. W.; White, H. S. Electrochemical Measurements of Single H 2 Nanobubble Nucleation and Stability at Pt Nanoelectrodes. *J. Phys. Chem. Lett.* **2014**, *5*, 3539−3544.
(27) Bashkatov, A.; Park, S.; Demirkır, Ç.; et al. Performance Enhancement of Electrocatalytic Hydrogen Evolution through Coalescence-Induced Bubble Dynamics. *J. Am. Chem. Soc.* **2024**, *146*, 10177−10186.
(28) Park, S.; Liu, L.; Demirkır, Ç.; et al. Solutal Marangoni effect determines bubble dynamics during electrocatalytic hydrogen evolution. *Nat. Chem.* **2023**, *15*, 1532−1540.
(29) van der Heijden, O.; Park, S.; Eggebeen, J. J. J.; Koper, M. T. M. Non-Kinetic Effects Convolute Activity and Tafel Analysis for the Alkaline Oxygen Evolution Reaction on NiFeOOH Electrocatalysts. *Angew. Chem., Int. Ed.* **2023**, *62*, No. e202216477.
(30) van der Heijden, O.; Park, S.; Vos, R. E.; Eggebeen, J. J. J.; Koper, M. T. M. Tafel Slope Plot as a Tool to Analyze Electrocatalytic Reactions. *ACS Energy Lett.* **2024**, *9*, 1871−1879.
(31) Corva, M.; Blanc, N.; Bondue, C. J.; Tschulik, K. Differential Tafel Analysis: A Quick and Robust Tool to Inspect and Benchmark Charge Transfer in Electrocatalysis. *ACS Catal.* **2022**, *12*, 13805−13812.
(32) Zoski, C. G. Ultramicroelectrodes: Design, fabrication, and characterization. *Electroanalysis* **2022**, *14*, 1041−1051.
(33) Liu, Y.; Edwards, M. A.; German, S. R.; Chen, Q.; White, H. S. The Dynamic Steady State of an Electrochemically Generated Nanobubble. *Langmuir* **2017**, *33*, 1845−1853.
(34) German, S. R.; Edwards, M. A.; Ren, H.; White, H. S. Critical Nuclei Size, Rate, and Activation Energy of H 2 Gas Nucleation. *J. Am. Chem. Soc.* **2018**, *140*, 4047−4053.
(35) German, S. R.; Edwards, M. A.; Chen, Q.; White, H. S. Laplace Pressure of Individual H 2 Nanobubbles from Pressure−Addition Electrochemistry. *Nano Lett.* **2016**, *16*, 6691−6694.
(36) Meulenbroek, A. M.; Vreman, A. W.; Deen, N. G. Competing Marangoni effects form a stagnant cap on the interface of a hydrogen bubble attached to a microelectrode. *Electrochim. Acta* **2021**, *385*, No. 138298.
(37) Yang, X.; Karnbach, F.; Uhlemann, M.; Odenbach, S.; Eckert, K. Dynamics of Single Hydrogen Bubbles at a Platinum Microelectrode. *Langmuir* **2015**, *31*, 8184−8193.
(38) Bashkatov, A.; Hossain, S. S.; Mutschke, G.; et al. On the growth regimes of hydrogen bubbles at microelectrodes. *Phys. Chem. Chem. Phys.* **2022**, *24*, 26738−26752.
(39) Park, S.; Bashkatov, A.; Eggebeen, J. J. J.; et al. Combined effects of electrode morphology and electrolyte composition on single H 2 gas bubble detachment during hydrogen evolution reaction. *Nanoscale* **2025**, *17*, 10020−10034, DOI: 10.1039/D5NR00234F.
(40) Toyama, K.; Kanemoto, R.; Misumi, R.; Araki, T.; Mitsushima, S. Faster R-CNN-based Detection and Tracking of Hydrogen and Oxygen Bubbles in Alkaline Water Electrolysis. *Electrochemistry* **2025**, *93*, 24−00127.
(41) Noskov, B. A. Fast adsorption at the liquid-gas interface. *Adv. Colloid Interface Sci.* **1996**, *69*, 63−129.
(42) Brandon, N. P.; Kelsall, G. H.; Levine, S.; Smith, A. L. Interfacial electrical properties of electrogenerated bubbles. *J. Appl. Electrochem.* **1985**, *15*, 485−493.
(43) Calgaroto, S.; Wilberg, K. Q.; Rubio, J. On the nanobubbles interfacial properties and future applications in flotation. *Miner. Eng.* **2014**, *60*, 33−40.
(44) Scheu, R.; Chen, Y.; Subinya, M.; Roke, S. Stern Layer Formation Induced by Hydrophobic Interactions: A Molecular Level Study. *J. Am. Chem. Soc.* **2013**, *135*, 19330−19335.
(45) Liu, B.; Manica, R.; Liu, Q.; et al. Nanoscale Transport during Liquid Film Thinning Inhibits Bubble Coalescing Behavior in Electrolyte Solutions. *Phys. Rev. Lett.* **2023**, *131*, No. 104003.
(46) Craig, V. S. J.; Ninham, B. W.; Pashley, R. M. The effect of electrolytes on bubble coalescence in water. *J. Phys. Chem. A* **1993**, *97*, 10192−10197.
(47) Park, S.; Lohse, D.; Krug, D.; Koper, M. T. M. Electrolyte design for the manipulation of gas bubble detachment during hydrogen evolution reaction. *Electrochim. Acta* **2024**, *485*, No. 144084.
(48) Kartikawati, N. A.; Safdar, R.; Lal, B.; Mutalib, M. I. B. A.; Shariff, A. M. Measurement and correlation of the physical properties of aqueous solutions of ammonium based ionic liquids. *J. Mol. Liq.* **2018**, *253*, 250−258.
(49) Wen, J.; Shi, K.; Sun, Q.; Sun, Z.; Gu, H. Measurement for Surface Tension of Aqueous Inorganic Salt. *Front. Energy Res.* **2018**, *6*, No. 12, DOI: 10.3389/fenrg.2018.00012.
(50) Fernández, D.; Maurer, P.; Martine, M.; Coey, J. M. D.; Möbius, M. E. Bubble Formation at a Gas-Evolving Microelectrode. *Langmuir* **2014**, *30*, 13065−13074.
(51) Monzon, L. M. A.; Gillen, A. J.; Mobius, M. E.; Coey, J. M. D. Effect of Tetraalkylammonium Cations on Gas Coalescence at a Hydrogen-Evolving Microelectrode. *Langmuir* **2015**, *31*, 5738−5747.
(52) Vannoy, K. J.; Renault, C.; Dick, J. E. The Microelectrode Insulator Influences Water Nanodroplet Collisions. *Anal. Chem.* **2023**, *95*, 7286−7293.

https://doi.org/10.1021/acscatal.5c08904
ACS Catal. 2026, 16, 5796−5804